Experimental application of orthogonal eigenstructure control for structural vibration cancellation

M.A. Rastgaar [a,b,*], M. Ahmadian [b], S.C. Southward [b]

[a] Department of Mechanical Engineering, Massachusetts Institute of Technology, 77 Mass ave. 3-147, Cambridge, MA 02139, USA
[b] Center for Vehicle Systems & Safety, Mechanical Engineering Department, Virginia Polytechnic Institute and State University, Blacksburg, VA 24061, USA

ABSTRACT

Orthogonal eigenstructure control (OEC) is a novel feedback control that is applicable to linear systems. Orthogonal eigenstructure control can minimizes the trial and error by the controller designer. It finds orthogonal vectors to some targeted modes of the structure within the achievable eigenvector set. When the targeted modes are replaced with the orthogonal vectors, it results in a decoupled system or structure that leads to vibration isolation. In this article, experimental application of this control method for active vibration cancellation of a plate is presented. Piezoelectric actuators are used as control actuators and accelerometers are used as feedback sensors. Vibration cancellation in a plate due to 150 Hz sinusoidal disturbance and a wideband disturbance within the range 200–300 Hz are experimentally studied. Since OEC is a model-based control method, system identification techniques are used for estimating the state-space realization of the system model. The effect of tuning the control gain is studied to compensate for the inaccurate system identification or factors that cannot be identified easily but play a major role in vibration of a structure. A finite element model of a plate is considered and the effects of scaling the control gains are investigated. It is shown that there is an allowable region for tuning the control gain without loosing the stability. The result of this analysis is used in the experiment for adjusting the control gains.

© 2010 Elsevier Ltd. All rights reserved.

1. Introduction

It has been shown that eigenstructure assignment methods are effective for active vibration cancellation in structures. The idea of eigenstructure assignment methods is similar to normal mode localization that divides a structure into two areas. Vibration isolation is confined to selected areas while no attempts are made to reduce vibration in other areas. Normal mode localization usually happens when one or more global modes of vibrations become confined to a local region of the structure. Material and structural discontinuity may generate a disorder in the periodicity of the structure; therefore, the vibrational energy cannot propagate into the structure thoroughly and will be confined to the areas that are closed to the source of vibrations [1,2]. For large space structures, localization can be used as a method of vibration confinement at the areas close to the source of disturbance [3]. It has been shown that methods based on vibration confinement reduce the amplitude of vibration much more effectively than other methods of vibration suppression [4,5]. Using the normal mode localization concept in periodic structures along with eigenstructure assignment approach, Song and Jayasuriya [5]

---

* Corresponding author at: Department of Mechanical Engineering, Massachusetts Institute of Technology, 77 Mass ave. 3-147, Cambridge, MA 02139, USA. Tel.: +1 617 253 8117; fax: +1 540 808 8766.
E-mail address: Rastgaar@mit.edu (M.A. Rastgaar).

proposed an algorithm for choosing a linearly independent set of mode shapes in order to reduce the relative vibrational amplitude at certain areas by redistributing the vibrational energy.

The possibility of assigning the eigenvectors during pole placement control was introduced by Moore [6] when he showed that there is a class of eigenvectors that can be assigned to a specific set of eigenvalues of a closed-loop state feedback system. A numerical approach to this problem was proposed by Cunningham [7], employing singular value decomposition to find the basis of the null space for achievable eigenvector set.

Shelly and Clark. [8,9] introduced eigenvector scaling, which is a mode localization technique called for regulating specific elements of eigenvectors to increase the relative displacement of the corresponding areas in the system. Validations of proposed method with piezoelectric transducers are reported in [10,11]. Since in practice state feedback is hardly achievable, SVD-eigenvector shaping has been developed by Shelly and Clark [12] to address the issue of limited pairs of actuators and sensors. The method that is experimentally evaluated here is a combination of the authors' earlier methods and the approach suggested by Cunningham. SVD-eigenvector shaping uses Moore–Penrose generalized left inverse. Since it minimizes Euclidean 2-norm error, it yields the closest eigenvector in least square sense to the desired ones.

Tang and Wang [13,14] used a hybrid vibration confinement system using a network of piezoelectric actuators and used the eigenstructure assignment to confine the vibrational energy to the passive elements of the electrical circuit integrated with the system. After finding the subspace for the eigenvectors, the optimal achievable eigenvectors that have the minimal vector 2-norm in concerned regions can be achieved. Using the passive circuitry elements as extra design variables, the system can be introduced as the one with larger dimension than the original system. Since suppression of vibrations is required for degrees of freedom associated with the mechanical parts of the system, while confining energy to the degrees of freedom associated with the electrical circuitry, a perfect match between the desired eigenvectors and the achievable ones is not necessary.

The eigenstructure assignment methods currently available, however, depend on the experience of the controller designer, based on the geometry and dynamics of the structures. Most of the existing methods require apriori definition of the desired eigenstructure. Identifying the desirable locations for the closed-loop eigenvalues and defining the desirable closed-loop eigenvectors are not a straightforward task. For large scale systems, it becomes impractical to define a desired closed-loop eigenstructure. Therefore, the existing methods are not able to be applied to such systems or many other similar practical engineering structures. Considering that there are no one-to-one relationships between the elements of the closed-loop eigenvectors and the states of the system, one may define desirable eigenvectors that do not satisfy a given design criterion. This may lead to excessive actuation forces because of improper location of the associated closed-loop poles. Additionally, the desirable eigenvectors do not necessarily lie within the space of achievable eigenvectors. The missing piece of this puzzle is a control method that can automatically lead to a set of desirable closed-loop eigenvectors, which result in mode decoupling and disturbance rejection.

A novel control method, namely orthogonal eigenstructure control, for vibration cancellation in structures was developed. This method is a feedback control method applicable to multiple-input multiple-output linear systems. This control method can determine the feedback control law with minimal experience of controller designer. This new structural vibration control method is able to perform robustly in the presence of a wide variety of disturbances, while significantly reducing the controller development cycle through a mathematically sound approach that can be implemented easily on a broad range of structures in practice.

OEC eliminates the need for defining the desirable eigenvectors and eigenvalues of the closed-loop system, which are usually required by other eigenstructure assignment methods. This significantly reduces the amount of time needed for developing a new controller for structural control. OEC is able to suggest a set of closed-loop systems. For open-loop eigenvectors associated with the operating eigenvalues, this method finds orthogonal vectors within the achievable eigenvector set and substitute them as the associated open-loop eigenvectors. The controller designer can easily determine the most desirable solution by assessing the performance of the results of a number of closed-loop systems for all possible systems. Progressive application of OEC makes the set of suggested closed-loop systems unbounded.

In this study, a test setup is used to evaluate the application of OEC for active vibration cancellation of a thin steel plate. Based on the characteristics of the test plate, the range of frequency of 200–300 Hz is considered as the frequency range of interest. The state space model of the system is identified using the Matlab System Identification Toolbox. Then, OEC is used for identifying the proper control gains that decouple the modes of the plate in order to suppress vibrations. Three different sets of experiments are performed. First, a tonal disturbance with a frequency of 150 Hz is applied to the plate. Second, a wideband disturbance with a frequency range of 200–300 Hz is used for inducing the vibrations to the plate. For both the aforementioned experiment, the control gains calculated by OEC are used with no adjustment. In the third experiment, again a wideband disturbance with the frequency range of 200–300 Hz is applied and the control gains are scaled up in order to compensate for un-modeled dynamics of the plate through the system identification process. A finite element model of the plate is used to study the adjustment of the control gains.

In this paper the theoretical aspects of OEC are described briefly. Then, a finite element model of a rectangular plate is used to show the applicability of the gain adjustment to compensate for dynamics of the system that has not been taken into account during system identification process. Experimental setup and test plate characteristics are described in detail. Next, the result of application of OEC for suppression of tonal disturbance and wideband disturbance with and without control gain scaling are followed. Finally the outcomes of the reported experiments are discussed.

2. Theoretical background

In this section, we briefly introduce the theory of orthogonal eigenstructure control. More detail discussions and proofs can be found in earlier publications by the authors [15–21]. Let us consider the equation of motion for a linear first-order system

$$\dot{\mathbf{x}} = \mathbf{Ax} + \mathbf{Bu} + \mathbf{Ef} \tag{1}$$

$$\mathbf{y} = \mathbf{Cx} \tag{2}$$

$$\mathbf{u} = \mathbf{Ky} \tag{3}$$

Assuming m collocated actuators and sensors and no feedthrough term, $\mathbf{A}$ is the $N \times N$ state matrix, $\mathbf{B}$ is the $N \times m$ input matrix, $\mathbf{E}$ is the $N \times 1$ disturbance input matrix, $\mathbf{f}$ is the disturbance vector, $\mathbf{u}$ is the input vector of dimension m, $\mathbf{y}$ is the $m \times 1$ output vector, and $\mathbf{C}$ is the $m \times N$ output matrix. The $m \times m$ feedback gain matrix $\mathbf{K}$ is sought that replaces targeted eigenvectors of the open-loop system with vectors orthogonal to them. Eqs. (1)–(3) can represent the following closed-loop system

$$\dot{\mathbf{x}} = (\mathbf{A} + \mathbf{BKC})\mathbf{x} + \mathbf{Ef} \tag{4}$$

where its eigenvalue problem is defined as

$$(\mathbf{A} + \mathbf{BKC})\boldsymbol{\phi}_i = \lambda_i \boldsymbol{\phi}_i \quad i = 1, 2, \ldots, N \tag{5}$$

$\boldsymbol{\phi}_i$ are the closed-loop eigenvectors of the system and λ_i are the eigenvalues. Eq. (5) can be written in a matrix form

$$[\mathbf{A} - \lambda_i \mathbf{I} | \mathbf{B}] \begin{Bmatrix} \boldsymbol{\phi}_i \\ \mathbf{KC}\boldsymbol{\phi}_i \end{Bmatrix} = 0 \quad i = 1, 2, \ldots, N \tag{6}$$

where $\mathbf{I}$ is the $N \times N$ identity matrix. The vector $\begin{Bmatrix} \boldsymbol{\phi}_i \\ \mathbf{KC}\boldsymbol{\phi}_i \end{Bmatrix}$ belongs to the null space of the matrix $\mathbf{S}_{\lambda i} = [\mathbf{A} - \lambda_i \mathbf{I} \quad |\mathbf{B}]_{N \times (N+m)}$. Applying singular value decomposition to $\mathbf{S}_{\lambda i}$ yields

$$\mathbf{S}_{\lambda i} = [\mathbf{U}_i]_{N \times N} [\boldsymbol{\Sigma}_i | \mathbf{0}_{N \times m}]_{N \times (N+m)} [\mathbf{V}_i^*]_{(N+m) \times (N+m)} \tag{7}$$

In OEC, the designer is not required to define the closed-loop eigenvalues for the system [15]. In fact, using the open-loop system model, one can identify the open-loop eigenvalues and use them in Eq. (6). They are called operating eigenvalues and the index i is used to specify the equation for the ith operating eigenvalue. The number of operating eigenvalues is the same as the number of the required pairs of actuators and sensors m. It has been shown that using the open-loop eigenvalues farthest away from the origin as the operating eigenvalues leads to a closed-loop system with reasonably desirable behavior [15,17,20]. $\mathbf{U}_i$ and $\mathbf{V}_i$ are the left and right orthonormal matrices respectively, and $\mathbf{V}_i^*$ is the conjugate transpose of the complex matrix $\mathbf{V}_i$. If $\mathbf{V}_i$ is partitioned, then the second column block of $\mathbf{V}_i$ spans the null space of $\mathbf{S}_{\lambda i}$ [4,15,17]

$$[\mathbf{V}_i]_{(N+m) \times (N+m)} = \begin{bmatrix} [\mathbf{V}_{11}^i]_{N \times N} & [\mathbf{V}_{12}^i]_{N \times m} \\ [\mathbf{V}_{21}^i]_{m \times N} & [\mathbf{V}_{22}^i]_{m \times m} \end{bmatrix} \tag{8}$$

Any linear combination of m columns of $\mathbf{V}_{12}^i$ is an achievable eigenvector of the closed-loop system; for a coefficient vector $\mathbf{r}^i$ it implies that

$$\boldsymbol{\phi}_i^a = \mathbf{V}_{12}^i \mathbf{r}^i \tag{9}$$

where $\boldsymbol{\phi}_i{}^a$ is an achievable eigenvector of the closed-loop system. The corresponding control gain matrix $\mathbf{K}$ can be found using

$$\mathbf{KC}\boldsymbol{\phi}_i^a = \mathbf{V}_{22}^i \mathbf{r}^i \tag{10}$$

Most of the eigenstructure assignment methods define a desired eigenvector for the system $\boldsymbol{\phi}_i{}^d$ using different approaches; however, they show a drawback that the controlled eigenvectors are not necessarily identical to the desired ones.

OEC regenerates the open-loop system by finding the open-loop eigenvectors and their orthogonal vectors for the operating modes. In other words, the open-loop eigenvectors of the operating modes are defined by the intersections of the open-loop eigenvector set and the achievable eigenvectors.

Using Eq. (9), we multiply the conjugate transpose of the ith achievable eigenvector by itself.

$$\mathbf{E}_i = \mathbf{r}^{i*} \mathbf{V}^* \mathbf{V}_{12}^i \mathbf{r}^i \tag{11}$$

Since $\mathbf{V}_{12}^i$ and $\mathbf{V}_{22}^i$ are complex matrices, $\mathbf{V}_{12}^i \mathbf{V}_{12}^i$ and $\mathbf{V}_{22}^i \mathbf{V}_{22}^i$ become Hermitian matrices and their eigenvalue decompositions yields

$$[\mathbf{V}_{12}^i]_{N \times m}^* [\mathbf{V}_{12}^i]_{N \times m} = \overline{\mathbf{U}}^i \overline{\boldsymbol{\Lambda}}^i \overline{\mathbf{U}}^{i*} \tag{12}$$

$$[\mathbf{V}_{22}^i]_{m \times m}^* [\mathbf{V}_{22}^i]_{m \times m} = \overline{\mathbf{U}}_w^i \overline{\boldsymbol{\Lambda}}_w^i \overline{\mathbf{U}}_w^{i*} \tag{13}$$

where $\overline{\boldsymbol{\Lambda}}^i$, $\overline{\mathbf{U}}^i$ and $\overline{\boldsymbol{\Lambda}}_w^i$, $\overline{\mathbf{U}}_w^i$ are the eigenvalue and eigenvector matrices of $\mathbf{V}_{12}^{i*}\mathbf{V}_{12}^i$ and $\mathbf{V}_{22}^{i*}\mathbf{V}_{22}^i$, respectively. It has been shown by the authors that the eigenvalues of the Hermitian products $\mathbf{V}_{12}^{i*}\mathbf{V}_{12}^i$ and $\mathbf{V}_{22}^{i*}\mathbf{V}_{22}^i$ belong to the $\begin{bmatrix} 0 & 1 \end{bmatrix}$ interval. It has also been shown that the eigenvectors of $\mathbf{V}_{22}^{i*}\mathbf{V}_{22}^i$ and $\mathbf{V}_{12}^{i*}\mathbf{V}_{12}^i$ are identical and the summation of the eigenvalues of $\mathbf{V}_{12}^{i*}\mathbf{V}_{12}^i$ and $\mathbf{V}_{22}^{i*}\mathbf{V}_{22}^i$ associated with similar eigenvectors are unity [15–17,19,21].

$$\overline{\boldsymbol{\Lambda}}_w^i + \overline{\boldsymbol{\Lambda}}^i = \mathbf{I} \tag{14}$$

$$\overline{\mathbf{U}}^i = \overline{\mathbf{U}}_w^i \tag{15}$$

If the eigenvector $\overline{\mathbf{U}}_J^i$ associated with a unity eigenvalue of $\mathbf{V}_{12}^{i*}\mathbf{V}_{12}^i$ is considered as $\mathbf{r}^i$ in Eq. (11), then $\mathbf{E}^i = 1$. Using this property, we re-arrange Eq. (12) to get

$$\overline{\mathbf{U}}^{i*}\mathbf{V}_{12}^{i*}\mathbf{V}_{12}^i\overline{\mathbf{U}}^i = \overline{\boldsymbol{\Lambda}}^i \tag{16}$$

If $\overline{\mathbf{U}}_J^i$ is the eigenvector corresponding to the unity eigenvalue of $\overline{\boldsymbol{\Lambda}}_i$, then

$$\overline{\mathbf{U}}_J^{i*}\mathbf{V}_{12}^{i*}\mathbf{V}_{12}^i\overline{\mathbf{U}}_J^i = 1 \tag{17}$$

$$\overline{\mathbf{U}}_J^{i*}\mathbf{V}_{22}^{i*}\mathbf{V}_{22}^i\overline{\mathbf{U}}_J^i = 0 \tag{18}$$

Combining Eqs. (17) and (18) yields

$$\mathbf{V}_{22}^i\overline{\mathbf{U}}_J^i = 0 \tag{19}$$

That results in

$$\mathbf{KC}\boldsymbol{\phi}_i^a = \mathbf{V}_{22}^i\mathbf{r}^i = \mathbf{V}_{22}^i\overline{\mathbf{U}}_J^i = 0 \tag{20}$$

or $\mathbf{K}=0$, which implies that the control gain $\mathbf{K}$ is zero. It means that the open-loop system is regenerated. The selected $\mathbf{r}^i$ generates the open-loop eigenvectors associated with the operating eigenvalue λ_i. $\mathbf{V}_{12}^i\overline{\mathbf{U}}_J^i$ is identical to the eigenvector corresponding to the operating eigenvalue. The other eigenvectors associated with non-unity eigenvalues of $\mathbf{V}_{12}^{i*}\mathbf{V}_{12}^i$ are orthogonal to the eigenvector associated with the unity eigenvalue of $\mathbf{V}_{12}^{i*}\mathbf{V}_{12}^i$. Therefore, a set of closed-loop eigenvectors can be found that are orthogonal to the open-loop eigenvectors.

Repeating this process for each pair of actuators and sensors, we append the calculated closed-loop eigenvectors for all operating eigenvalues and define $\mathbf{V}$ and $\mathbf{W}$ matrices as

$$\mathbf{V} = [\mathbf{V}_{12}^1\mathbf{r}^1 \cdots \mathbf{V}_{12}^m\mathbf{r}^m] \tag{21}$$

$$\mathbf{W} = [\mathbf{V}_{22}^1\mathbf{r}^1 \cdots \mathbf{V}_{22}^m\mathbf{r}^m] \tag{22}$$

The feedback gain matrix $\mathbf{K}$ is determined as

$$\mathbf{K} = \mathbf{W}(\mathbf{CV})^{-1} \tag{23}$$

Generally, for a system of collocated actuators and sensors $\mathbf{C}$ is a full-rank matrix. $(\mathbf{CV})^{-1}$ exists if $\mathbf{CV}$ is a square and nonsingular matrix. It requires $\mathbf{C}$ to be a full-rank matrix, since $\mathbf{V}$ can be defined as a full-rank matrix. The state matrix of the closed-loop system is

$$\mathbf{A_c} = \mathbf{A} + \mathbf{BKC} \tag{24}$$

As stated in [15,16,19,21], the number of possible closed-loop systems upon application of OEC is $m^m - 1$, where m is the number of actuators or sensors—in the case of equal number of actuators and sensors. The control gain matrix with the most desirable performance – reduced vibration amplitude in this paper – should be selected as the outcome of the controller design. Moreover, progressive application of OEC [15] ensures achieving a stable closed-loop system.

3. Simulation and analysis

As an example of a system with large degrees of freedom, a plate that is clamped along its four edges is considered and the orthogonal eigenstructure control is used to suppress the vibrations induced by a point source of disturbance. The plate is assumed to be a rectangular steel plate of the size 400 by 500 mm and thickness of 1 mm. The Young's modulus of the material is $2.09 \times 10^9\,\mathrm{N/m^2}$ and the Poisson's ratio is 0.31. The plate is modeled using finite element analysis assuming Mindlin plate theory to include the transverse shear deformation in the definition of the plate displacement field [22]. This is the model of the plate that we later use in the experiments. Matlab is used for simulating the plate dynamics. Fig. 1 shows the plate, the assigned nodes, and its identical rectangular elements.

The procedures for determining the local mass and stiffness matrices are reported in [22]. Linear quadrilateral elements are used to model the plate. Each node has three degrees of freedom, including two in-plane displacements in x and y directions and a transverse displacement along z axis. Since the model consists of 49 nodes, the dimensions of the global
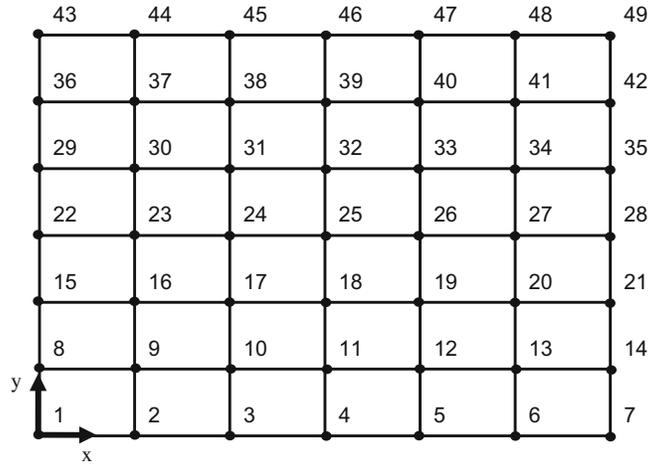
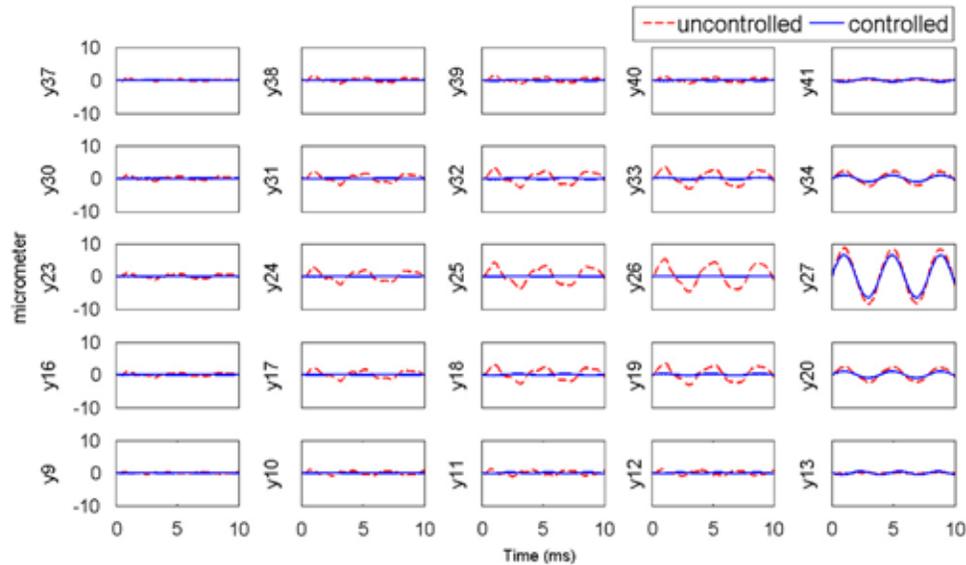**Fig. 1.** Nodes of the rectangular plate clamped at four edges.

Fig. 2. Comparison of displacements at different nodes of plate with and without control.

mass and stiffness matrices are 149×149, while the dimension of the state matrix is 298×298. The system is assumed to have linear damping.

A transverse sinusoidal input with a frequency of 250 Hz is applied to the plate at node 27 to study the dynamic behavior of the plate. Fig. 2 depicts the vibrations at different nodes of the plate. The nodes on the boundaries are not shown in this figure since they have zero displacements. There are two piezoelectric actuators at nodes 25 and 26. Table 1 shows the percentage of reduction of the maximum amplitude of vibrations, indicating that nodes 25 and 26 are isolated almost 100 percent.

Fig. 2 shows that the actuators have a localized effect on the nodes to which they are mounted and also the ones close to them. Note that for this simulation, input and output matrices, **B** and **C**, are considered sparse matrices assuming that the actuators apply to this local nodes only. This situation, however, is far from reality for laboratory tests. Because OEC is a model-based control, its application needs employing system identification techniques to estimate a state space model for plate and control system. The system identification results in a state space model with populated **B** and **C** matrices. Also, the accuracy of the system identification techniques may influence the outcome of the control algorithm. Therefore, in the next section we study the effects of scaling the control gain matrix determined by the orthogonal eigenstructure control.

4. Effects of scaling the control gain matrix

Often in control practice the overall control gain matrix is scaled up or down in order to compensate for the effect of uncounted parameters. System identification algorithms are used to estimate a model for the structures such as our test plate. Since orthogonal eigenstructure control is a model-based control method, the major source of uncertainty is an inaccurate model of the system. In order to assess the effects and limits of scaling the control gain matrix determined by orthogonal eigenstructure control, we consider the finite element model of the plate shown in Fig. 1. The disturbance, similar to the previous section, is a 250 Hz sinusoidal input applied to node 27 and the piezoelectric control actuators are located at nodes 25 and 26. Choosing the same open-loop eigenvalues as those in the previous section as the operating eigenvalues, we can calculate the control gain matrix accordingly.

The control gain is multiplied by 1/10, 1/3, 1/2, 2, and 3 and the maximum amount of the displacements at different nodes along with the change in the closed-loop pole locations are compared. Table 2 presents the peak amplitude change at plate nodes when the control gains are scaled up and down. It shows that scaling up the control gain matrix with factors of 2 and 3 slightly offset vibrations at most nodes, except for nodes 25 and 26 that are affected significantly and nodes 17, 24, and 31, which are affected moderately. This is attributed to the close proximity of nodes 17, 24, and 31 to the control actuators.

Scaling down the control gain matrix by 1/2 and 1/3 yield a reverse effect. Scaling down the gain matrix by a factor of 1/10 decreases vibration reduction significantly, while scaling up by a factor of 3.6 leads to more vibrations. Fig. 3 depicts the pole plots of the closed-loop systems with different control gains.

Fig. 4 shows the pole plots of the controlled plate with different overall gains. Scaling down the control gain matrix causes the two closed-loop poles that moved away from the loci of the open-loop poles to come closer to the loci and eventually they merge with the loci if the control gain is scaled down further. On the other hand, those poles move away from the open-loop poles loci when the control gain matrix is scaled up. When the overall gain is multiplied by 2 and 3, the locations of new poles imply less damping. As such, when the overall control gain is multiplied by 3.6, the vibrations become large.

It is important to note that we are not trying to define the allowable span for the scaling factors. We, however, would like to demonstrate that tuning the control gain matrix by scaling is permitted as long as the scaling does not exceed certain limits. This addresses the need for tuning the control gains in practical application of orthogonal eigenstructure control, when the accuracy of the system model is dependent on the system identification methods that are used.

Table 1
Reduction percentage of the maximum amplitude of vibrations at different nodes of plate.

Nodes	Reduction percentage (%)	Nodes	Reduction percentage (%)
9, 37	79	19, 33	90
10, 38	91	20, 34	60
11, 39	77	23	90
12, 40	77	24	96
13, 41	55	25	99
16, 30	94	26	99
17, 31	96	27	10
18, 32	92		

Table 2
Percentage of change in maximum amplitude of vibrations for different scale factors relative to the baseline.

| Nodes	Scale 1/10	Scale 1/3	Scale 1/2	Scale 2	Scale 3
9, 37	25.52	5.35	2.69	−1.52	−2.04
10, 38	10.53	2.92	1.51	−0.81	−1.09
11, 39	−5.35	−0.52	−0.20	0.07	0.10
12, 40	−16.32	−1.72	−0.69	0.32	0.39
13, 41	−1.82	0.16	0.11	−0.12	−0.12
16, 30	48.74	−1.81	−1.02	0.57	0.78
17, 31	34.14	12.14	6.51	−3.59	−4.84
18, 32	−12.60	−1.47	−0.72	0.25	0.36
19, 33	42.77	8.80	4.02	−2.06	−2.76
20, 34	10.91	2.78	1.45	−0.74	−0.98
23	18.40	1.73	0.66	−0.18	−0.22
24	117.27	33.99	17.63	−9.31	−12.49
25	446.94	164.22	86.97	−48.22	−65.07
26	774.99	190.30	97.19	−49.60	−66.30
27	2.09	0.622	0.31	−0.15	−0.20
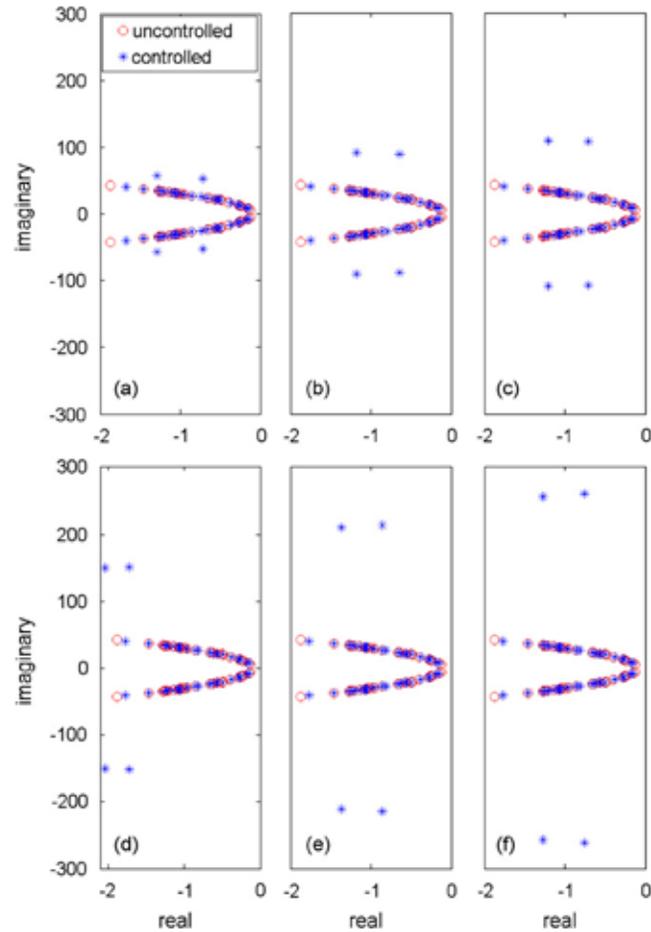
Fig. 3. Partial pole plots of controlled plate with different gain scale factors: (a) scale factor 1/10, (b) scale factor 1/3, (c) scale factor 1/2, (d) no scale factor, (e) scale factor 2, and (f) scale factor 3.

5. Experimental setup

A standard 20-gauge galvanized steel test plate, shown in Fig. 4, is used for evaluating the applicability of orthogonal eigenstructure control. This plate is clamped to the frame using 14 bolts that are tightened to a torque of 25 Nm. The test area of the plate is 500×400 mm with 50 mm of clamped length on each edge making the total dimensions 600×500 mm.

The electromagnetic actuator that is used for applying the disturbance input to the plate is part of a P1906 Linear Vibration Apparatus manufactured by Cussons Technology. An axially-stiff stinger made of a threaded rod is used to connect the actuator to the plate. At the tip of the stinger a Nylon spacer is placed and glued to the plate to provide a smooth contact area. The stinger is glued 85 mm from the right edge of the plate, on the axis of symmetry of the short side. The drive unit amplifier of the P1906 Linear Vibration Apparatus can be driven by an external oscillator and may be regarded as an operational amplifier with a voltage gain of unity from DC to 10 kHz.

Two high performance piezoelectric actuators T234-A4CL-503 $\times$ from Piezo systems, Inc. are used as control actuators. The piezoceramic control actuators (2.5×1.25 in) are composite reinforced bending bimorphs made of PSI-5A4E, with thickness of 0.034 in. It is cross poled for series bending operation, requiring two wires for upper and lower surfaces. Each piezoceramic actuator weighs 9.7 g and has rated voltage of ± 250 V. One of the piezoelectric actuators is placed at the center of the plate, the other one is at 100 mm away from the first one along the long side of the plate. The distance between the second piezoelectric actuator and the electromagnetic actuator is 85 mm.

A two channel non-inverting high-voltage piezo driver (amplifier) PZD700 manufactured by Trek is used to provide control signals to the piezoelectric actuators. The output voltage of the piezo driver is within 0 to ± 700 V with a current range of 0 to ± 100 mA. The amplifier has an adjustable output gain 0–300 V/V, and has a signal bandwidth of greater than 50 kHz for all voltage ranges.

PCB accelerometers, model U352L65 ICP with nominal sensitivity of 100 mV/g, are used to measure the acceleration at 10 locations of the plate. Seven accelerometers are placed on the top surface of the test plate, with three accelerometers
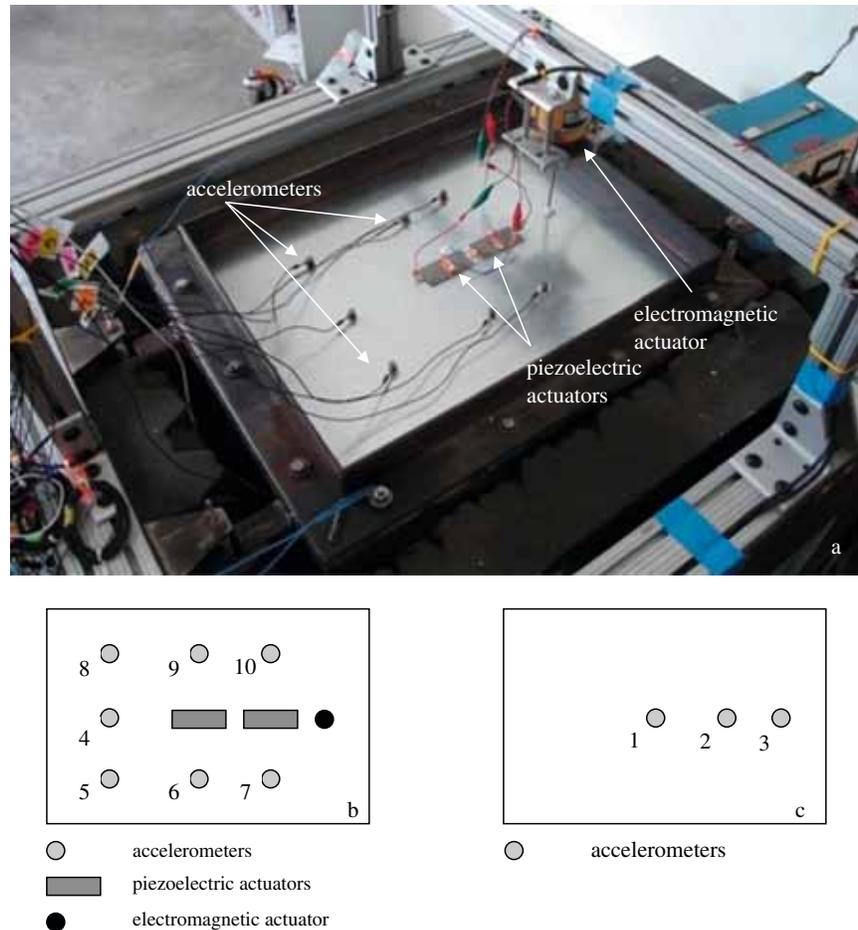
Fig. 4. Test set up: (a) test plate mounted on the frame structure, (b) schematic of the top view of plate, and (c) schematic of the bottom view of plate.

(Nos. 1, 2, and 3) collocated with the two control and disturbance actuators are mounted on opposite side as shown in Fig. 4b and c. The accelerometers are equally spaced in the transversal direction about 100 mm apart. A 20 channel ICP 584 series signal conditioner from PCB Piezotronics, Inc. is used with each channel gain set to 100.

Matlab System Identification Toolbox provides the prediction-error minimization algorithm [23], which is used for system identification to find the state space model of the test plate. For our experiment, the plate model is identified using the test data when the piezoelectric actuators are used as the source of input to the plate. The data collected from the sensors collocated with the piezoelectric actuators are used for system identification. This method finds the transfer functions for the command signals to each piezoelectric actuator as well as the transfer function between the command signals and the accelerometers collocated with the piezoelectric actuators. It then provides a first-order realization of the system model from the calculated transfer functions.

Fig. 5 shows the frequency response of the displacement at the center of the plate where accelerometer 1 is located to the signals from the accelerometer 3 that is collocated with the disturbance force. A proportional relationship between the disturbance force and the acceleration at the point of application is assumed. Fig. 5 shows coherence of almost 100 percent between the input and output signals in the range 150–300 Hz. Because the goal of this study is to validate the applicability of OEC, we will examine the application of a tonal disturbance at 150 Hz, and a wideband disturbance within the frequency range of 200–300 Hz.

6. Control of tonal disturbance

A tonal disturbance with a frequency of 150 Hz and amplitude of 1.5 mm is applied to the plate through the electromagnetic actuator. The integrated and filtered data from accelerometers 1 and 2 were collected for 6 s at 3000 Hz sampling rate. A tenth-order state space model of the system is estimated and orthogonal vibration control is applied to this estimated model to calculate the control gains. Fig. 6 shows plate vibration at the accelerometer locations. Upon
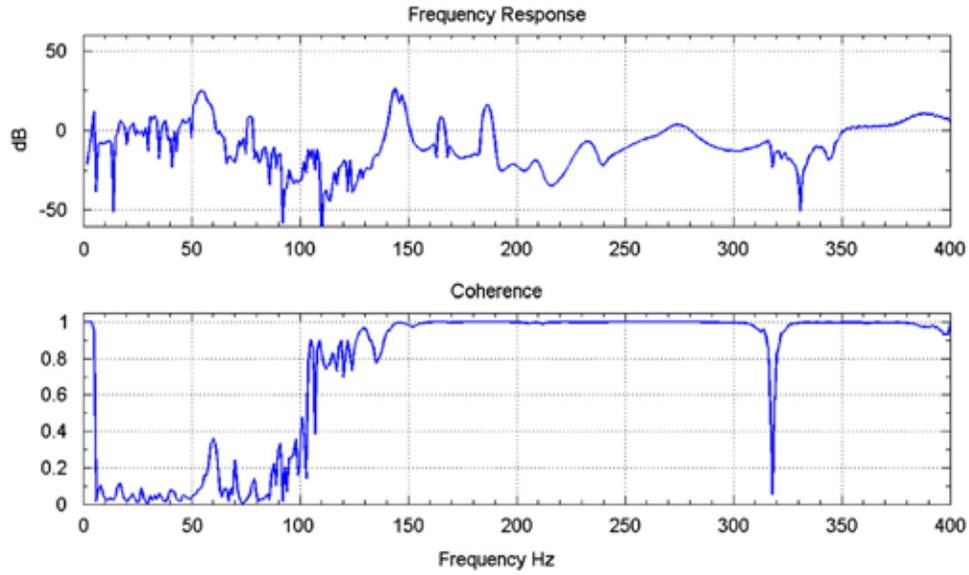
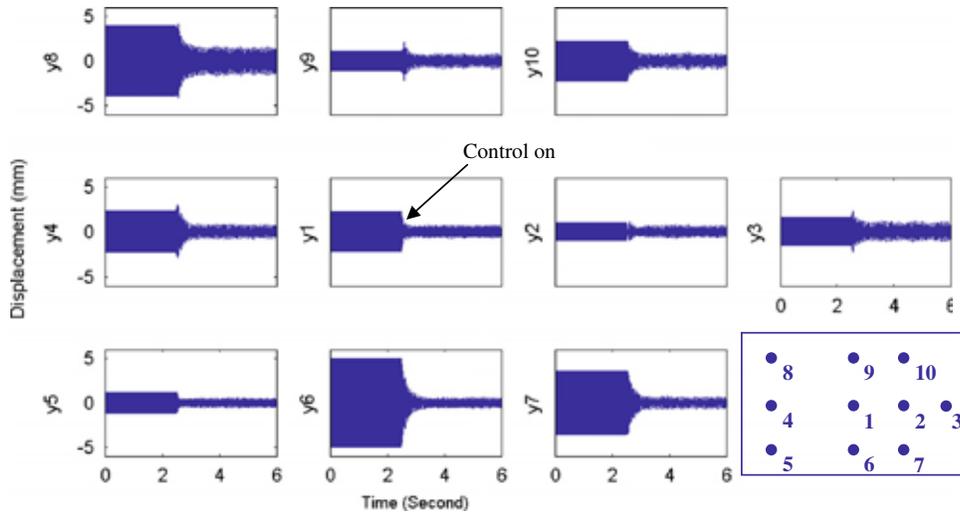**Fig. 5.** Frequency response and associated coherence at the center of plate.

Fig. 6. Displacement (mm) for control of 150 Hz disturbance with amplitude of 1.5 mm at accelerometer locations (150 Hz tonal disturbance). Control turned on after 2 s.

Table 3
Comparison of maximum displacement at accelerometer locations before and after controller is turned on (150 Hz pure tone with 1.5 mm amplitude disturbance).

Accelerometer	Maximum OL measurement	Maximum CL measurement	Percentage reduction (%)
1	2.27×10^{-3}	7×10^{-4}	-69
2	1.01×10^{-3}	7.29×10^{-4}	-28
3	1.51×10^{-3}	1.1×10^{-3}	-29
4	2.33×10^{-3}	7.88×10^{-4}	-66
5	1.19×10^{-3}	5.59×10^{-4}	-53
6	5×10^{-3}	5.75×10^{-4}	-88
7	3.59×10^{-3}	7.51×10^{-4}	-79
8	3.98×10^{-3}	1.53×10^{-3}	-62
9	1.12×10^{-3}	8.1×10^{-4}	-28
10	2.23×10^{-3}	8.27×10^{-4}	-63

turning on the controller at $t=2.5$ s, vibration reduced in the range of 28–88 percent at various locations as is shown in Table 3. The average vibration reduction across the plate is 57 percent.

7. Control of wideband disturbances

This section describes two tests that are conducted with a wideband disturbance in the frequency range of 200–300 Hz. The results complement those presented in the earlier section by showing the capability of the controller for reducing wideband vibrations. In the first experiment, the control gain matrix is determined using orthogonal eigenstructure control and used directly for control purposes. In the second experiment, the same control gain by an overall tuning factor 2 is used to compensate for the dynamics that are not considered in system identification process.

A sine sweep is used to simulate a wideband disturbance in the range 200–300 Hz with peak amplitude of 1 mm. The sweep duration is 30 s and it is repeated until the test is stopped. Fig. 7 shows the change in vibration amplitude at different accelerometer locations in time domain; similarly Fig. 8 depicts the control voltages to the piezoelectric actuators vs. time.

Figs. 9 and 10 present the comparisons between the frequency responses at accelerometers 1 and 2 to the disturbance signals, respectively. Significant vibration isolation is achieved in the frequency range of 200–270 Hz using orthogonal eigenstructure control. The shaded area in Fig. 9 indicates the frequency range with less isolation. Since the plate has a natural frequency at 273 Hz, vibrations are reduced less at 270 Hz and beyond as compared to the frequency range of
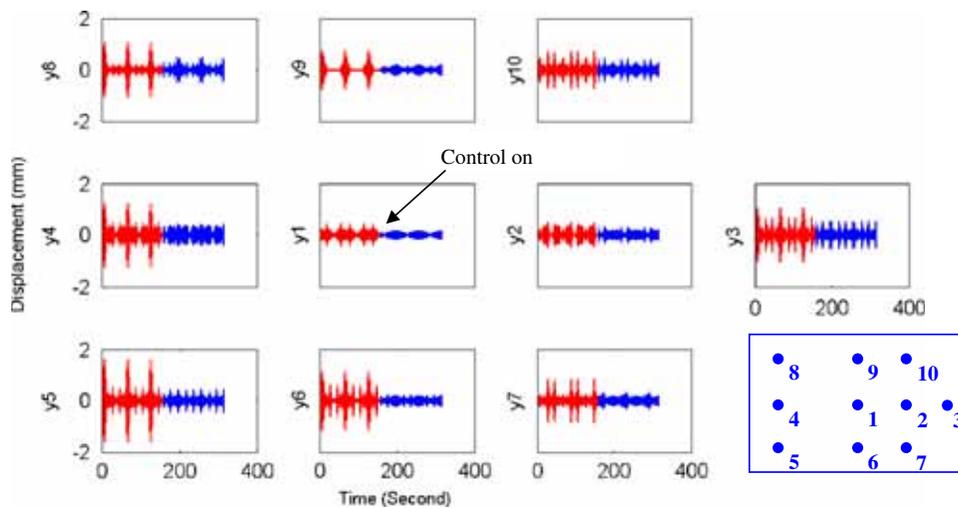

Fig. 7. Displacement (mm) at accelerometer locations; before and after control (200–300 Hz sine sweep disturbance).
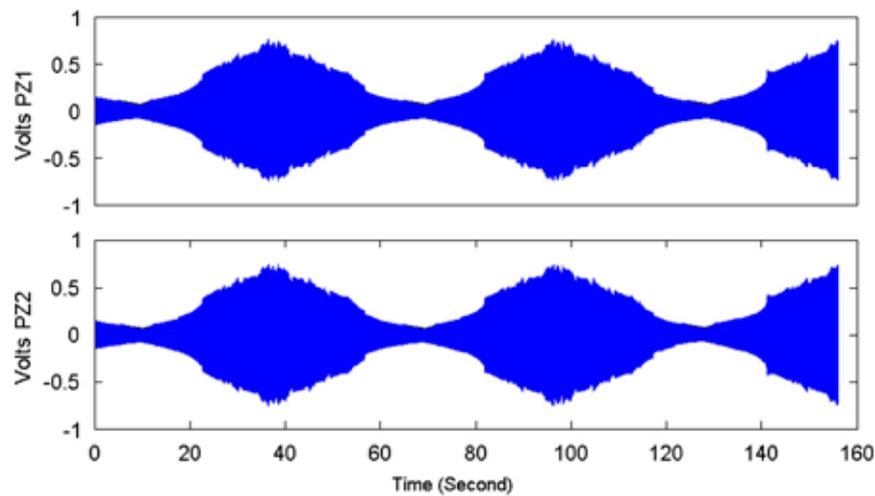

Fig. 8. Signals to the actuators (volts); PZ1: piezoelectric actuator at center of plate; and PZ2: piezoelectric actuator at off-center of plate (200–300 Hz sine sweep disturbance).
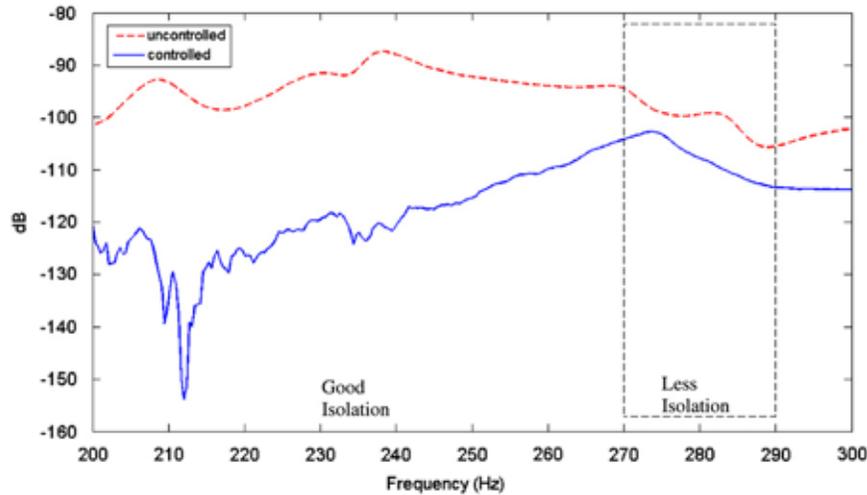
Fig. 9. Frequency responses to the sine sweep disturbance at accelerometer 1 (200–300 Hz sine sweep disturbance).
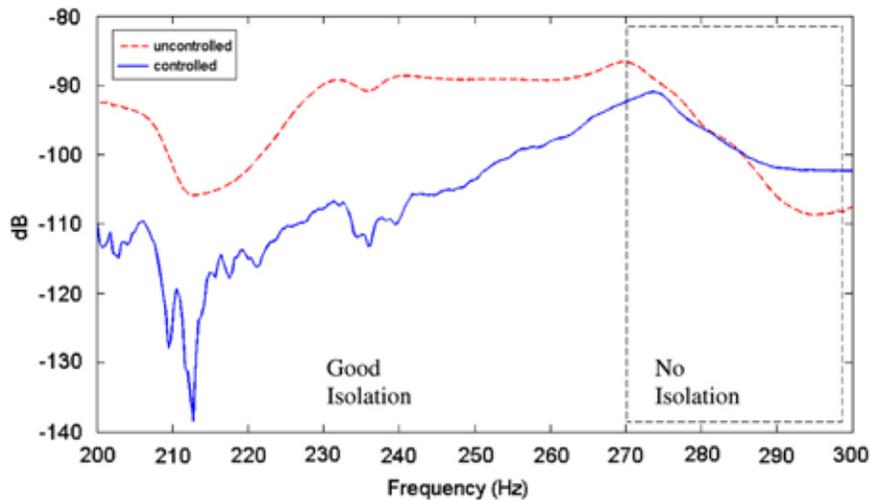

Fig. 10. Frequency responses to the sine sweep disturbance at accelerometer 2 (200–300 Hz sine sweep disturbance).

200–270 Hz. The same is observed for the accelerometer 2, as shown in Fig. 10 except that isolation is not achieved beyond 275 Hz and the amplitude of vibrations at accelerometer 2 is increased when the control is applied. One possible explanation for what is observed in Figs. 9 and 10 is that the actuators, in particular the one collocated with accelerometer 2, do not have enough authority to control the mode shape at 273 Hz.

Fig. 11 presents the ratio between the frequency responses of the controlled system to the uncontrolled system. In Fig. 11, amplitudes below 0 dB represents reduction in the magnitude of the response. The lowest reductions are observed in the range of 270–290 Hz. As stated before, this is partly because of the natural frequency that is at 273 Hz and limited authority of the actuators at this frequency. To address this issue, we examine adjusting the control gain to determine if it would be possible to achieve more isolation across a broader frequency range.

Repeating the experiment with the overall control gain matrix doubled increases vibration isolation across a broad frequency range. Doubling the gain matrix is intended to compensate for the effects to which the 273 Hz natural frequency is not represented in the system identification.

Fig. 12 shows the time trace for different accelerometers. Fig. 13 depicts the control voltages supplied to the piezoelectric actuators. As compared to Fig. 8, Fig. 13 shows significant increases in command voltage to the control actuators.

Figs. 14 and 15 show the frequency response for accelerometers 1 and 2 due to 100–300 Hz sine sweep disturbance. Doubling the overall control gain increases the isolation at higher frequencies. beyond 270 Hz. It shows that the increased gain reduces the effect of the natural frequency of plate at 273 Hz on the frequency response plots. Both accelerometers 1 and 2 show good isolation across the entire frequency range.
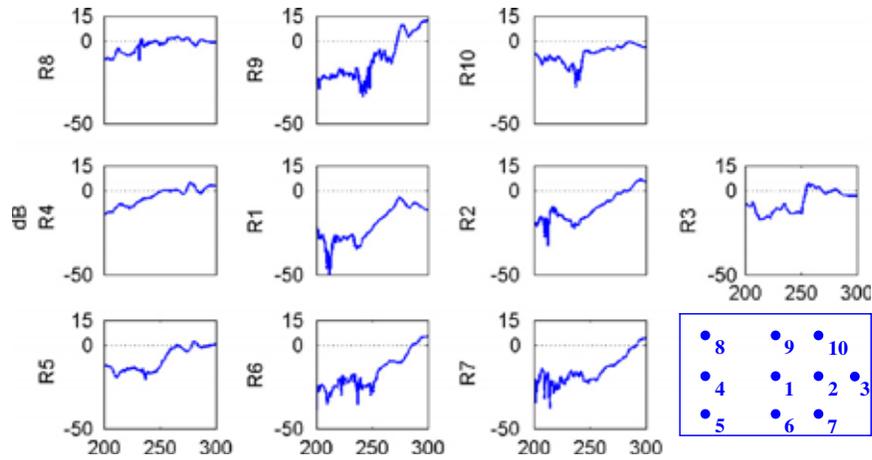
Fig. 11. Ratio of frequency response to the sine sweep disturbance of controlled system to uncontrolled system at various accelerometers (200–300 Hz sine sweep disturbance).
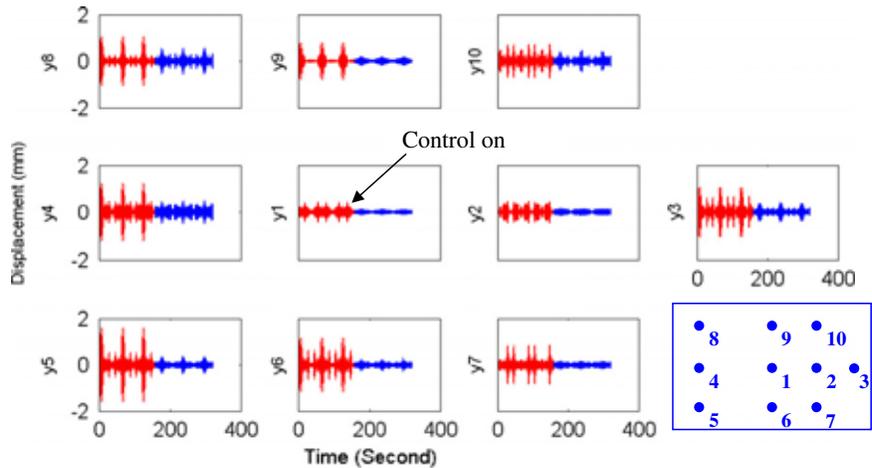

Fig. 12. Displacement (mm) at accelerometer locations; before and after control (200–300 Hz sine sweep disturbance).
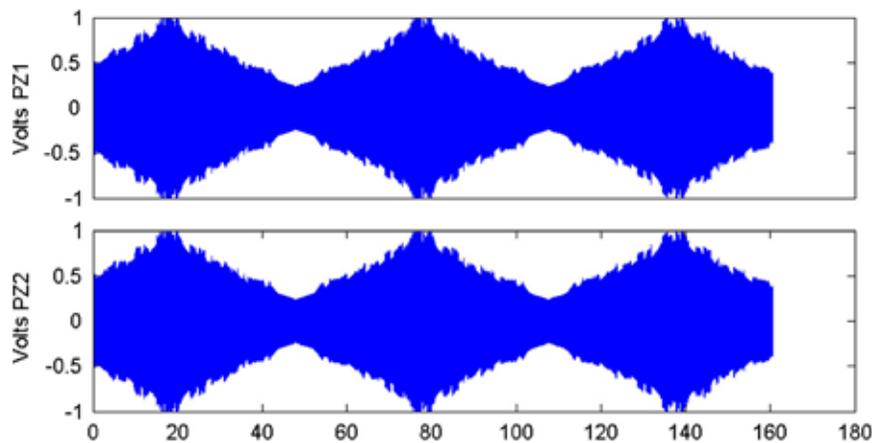

Fig. 13. Voltage provided to control actuators; PZ1: piezoelectric actuator at center of plate; and PZ2: piezoelectric actuator at off-center of plate (200–300 Hz sine sweep disturbance).
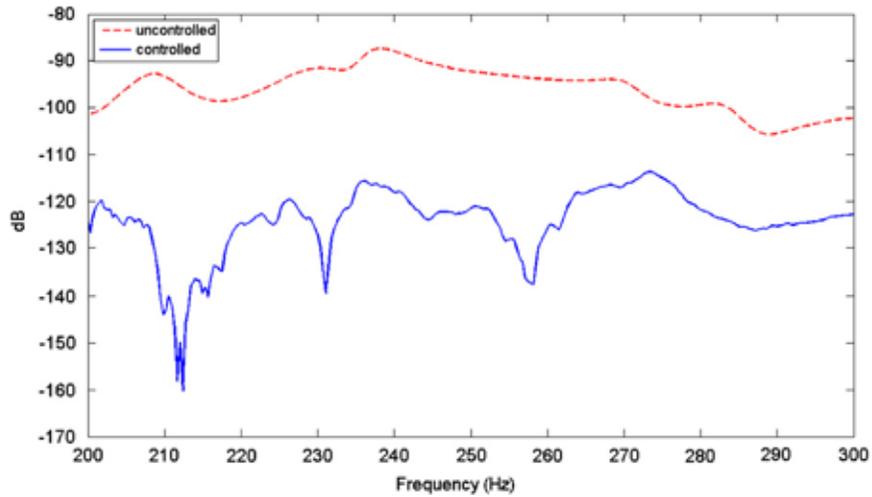
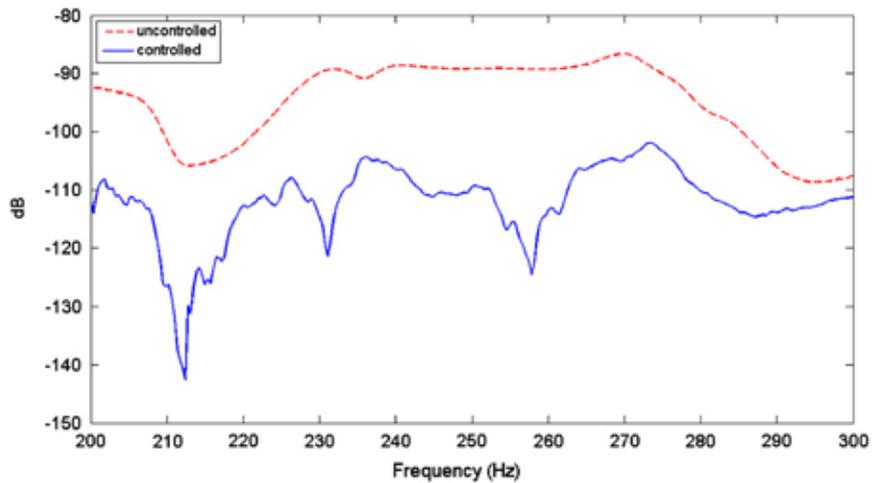**Fig. 14.** Frequency responses for accelerometer 1 (200–300 Hz sine sweep disturbance).

Fig. 15. Frequency responses for accelerometer 2 (200–300 Hz sine sweep disturbance).
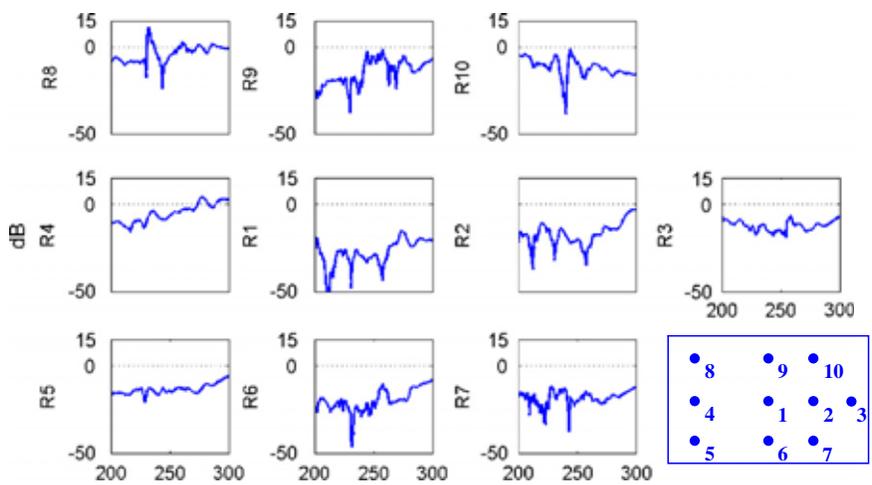

Fig. 16. Frequency response ratio between the controlled and uncontrolled system at various accelerometers (200–300 Hz sine sweep disturbance).
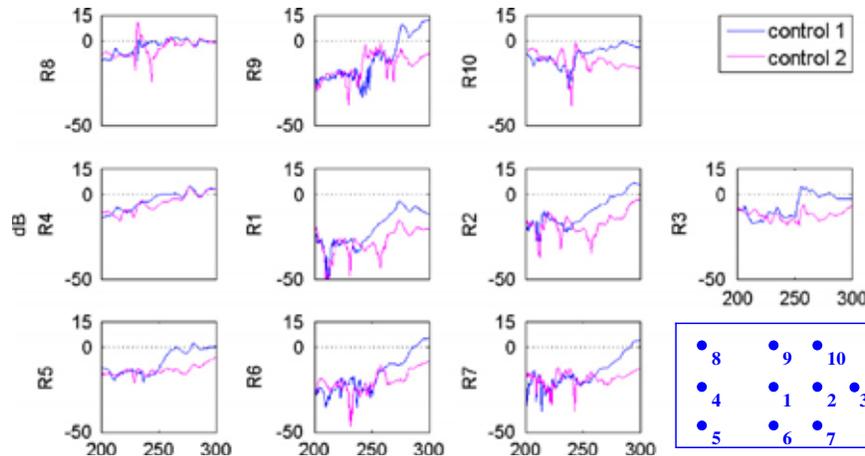
Fig. 17. Ratio of frequency response to the sine sweep disturbance of controlled system to un-controlled system at various accelerometers with two different control gains (comparison of Figs. 16 and 11), (200–300 Hz sine sweep disturbance).

Fig. 16 provides the ratio between the frequency responses of the controlled and uncontrolled system for the broadband sine sweep. Values below 0 dB present a reduction in the frequency response magnitude. Significant reduction in the frequency responses is achieved across the entire frequency range of 200–300 Hz, except at accelerometers 4 and 8. Fig. 17 shows a comparison of the two frequency response ratios between the current experiment and the previous one. It is clear that increasing the control gain compensates for estimation inherent in system identification results and factors that may not have been adequately represented in the model.

8. Conclusions

Orthogonal eigenstructure control was used for active vibration cancellation in a plate. Two piezoelectric bimorphs were used as control actuators and ten accelerometers were used for measuring vibrations. A series of experiments in vibration suppression due to a tonal disturbance at 150 Hz and a wideband disturbance of 200–300 Hz were performed. Since the orthogonal eigenstructure control is a model-based control method, system identification was used for estimating the state space realization of the structure and hardware. It was shown analytically that scaling the control gain compensates for estimation inherent in system identification and any factor not sufficiently presented in the model. The control gains can be calculated using the orthogonal eigenstructure control. The result of this analysis was used to achieve a better isolation across the entire range of frequency of the disturbance.

The orthogonal eigenstructure control holds great promise for significantly reducing structural vibrations with relatively minimal amount of trial and error by the controller designer in selecting the control parameters. This control method automatically replaces targeted modes of the system with orthogonal eigenvectors that are within the achievable eigenvector set and generate a closed-loop system with decoupled mode. Decoupling the modes of the system reduces spillover and provides increased vibration isolation.

References

[1] O.O. Bendiksen, Mode localization phenomena in large space structures, *AIAA Journal* 25 (9) (1987) 1241–1248.
[2] C.H. Hodges, J. Woodhouse, Confinement of vibration by structural irregularity, *Journal of the Acoustical Society of America* 69 (1) (1981).
[3] C. Pierre, P.D. Cha, Strong mode localization in nearly periodic disordered structures, *AIAA Journal* 27 (2) (1989) 227–241.
[4] F.J. Shelley, W.W. Clark, Experimental application of feedback control to localize vibration, *Journal of Vibration and Acoustics* 122 (2000) 143–150.
[5] B.Song, S. Jayasuriya, Active vibration control using eigenvector assignment for mode localization, *Proceedings of the American Control Conference*, San Francisco, California, 1993, pp. 1020–1024.
[6] B.C. Moore, On the flexibility offered by state feedback in multivariable systems beyond closed loop eigenvalue assignment, *IEEE Transactions on Automatic Control* 1 (1976) 689–692.
[7] T. B. Cunningham, Eigenspace selection procedures for closed loop response shaping with modal control, *Proceedings of the 19th IEEE Conference on Decision and Control*, Albuquerque, New Mexico, 1980, pp. 178–186.
[8] F. J. Shelley, W. W. Clark, Closed-loop mode localization for vibration control in flexible structures, *Proceedings of the American Control Conference*, Baltimore, Maryland, 1994, pp. 1826–1830.
[9] F.J. Shelley, W.W. Clark, Eigenvector scaling for mode localization in vibrating systems, *Journal of Guidance, Control, and Dynamics* 19 (6) (1996) 1342–1348.
[10] L.R. Corr, W.W. Clark, Vibration confinement using piezoelectric transducers and eigenstructure placement, *AIAA Journal* (1999) 99–1552.
[11] L.R. Corr, W.W. Clark, Active and passive vibration confinement using piezoelectric transducers and dynamic Vibration absorbers, *Proceedings of the SPIE Conference on Smart Structures and Integrated Systems*, Newport Beach, California, 3668, 1999, pp. 747–758.
[12] F.J. Shelley, W.W. Clark, Active mode localization in distributed parameter systems with consideration of limited actuator placement, part 2: simulations and experiments, *Journal of Vibration and Acoustics* 122 (2000) 165–168.

[13] J. Tang, K. W. Wang, A simultaneous active-aassive approach for structural vibration confinement using piezoelectric actuators, *Proceedings of the 44th AIAA/ASME/ ASCE/AHS Structures, Structural Dynamics, and Materials Conferences,* Norfolk, Virginia, 2003, pp. 1–11.

[14] J. Tang, K.W. Wang, Vibration confinement via optimal eigenvector assignment and piezoelectric networks, *Journal of Vibration and Acoustics* 126 (2004) 27–36.

[15] M. Rastgaar Aagaah, Vibration Suppression using Orthogonal Eigenstructure Control, PhD Dissertation, Virginia Polytechnic Institute and State University, Blacksburg, Virginia, USA, 2008.

[16] M.A. Rastgaar, M. Ahmadian, S.C. Southward, Orthogonal eigenstructure control for vibration suppression, *Journal of Vibration and Acoustics* 132 (1) (2010) 1–10.

[17] M. A. Rastgaar, M. Ahmadian, S. C. Southward, Vibration confinement by minimum modal energy eigenstructure assignment, *Proceedings of the ASME International Design Engineering Technical Conferences*, IDETC/CIE 2007, Las Vegas, Nevada, 2007.

[18] M. A. Rastgaar, M. Ahmadian, S. C. Southward, Effect of the actuators' location on vibration confinement using minimum modal energy eigenstructure assignment, *Proceedings of the ASME International Design Engineering Technical Conferences*, IDETC/CIE 2007, Las Vegas, Nevada, USA, 2007.

[19] M.A. Rastgaar, M. Ahmadian, S.C. Southward, Orthogonal eigenstructure control with non-collocated actuators and sensors, *Journal of Vibration and Control* 15 (7) (2009) 1019–1047.

[20] M. A. Rastgaar, M. Ahmadian, S. C. Southward, application of orthogonal eigenstructure control to flight control design, *Proceedings of the SPIE Smart Structures and Materials & Nondestructive Evaluation and Health Monitoring*, San Diego, CA, 2008.

[21] M. A. Rastgaar,, M. Ahmadian, S. C. Southward, Actuators' Locations in Vibration Cancellation of a Plate Using Orthogonal Eigenstructure Control, *Proceedings of the 18th. International Symposium on Mathematical Theory of Networks and Systems (MTNS08)*, Blacksburg, VA. 2008.

[22] W. Weaver, P.R. Johnston, *Structural Dynamics by Finite Element*, Prentice-Hall, 1987.

[23] L. Ljung, *System Identification: Theory for the User*, Prentice-Hall, Englewood Cliffs, NJ, 1987.